# Influence of the substrate on the phase composition and electrical properties of 0.65PMN–0.35PT thick films

H. Uršič [a,*], M. Hrovat [a], J. Holc [a], J. Tellier [a], S. Drnovšek [a], N. Guiblin [b], B. Dkhil [b], M. Kosec [a]

[a] *Electronic Ceramics Department, Jožef Stefan Institute, Jamova 39, SI-1000 Ljubljana, Slovenia*
[b] *Laboratoire Structures Proprietes et Modelisation des Solides, CNRS-UMR8580, Ecole Centrale Paris, Grande Voie des vignes, 92925 Chatenay-Malabry, France*

## Abstract

Thick films with the nominal composition $0.65Pb(Mg_{1/3}Nb_{2/3})O_3$–$0.35PbTiO_3$ (0.65PMN–0.35PT) were produced by screen-printing and firing paste prepared from an organic vehicle and pre-reacted powder. The films were fired for 2 h at 950 °C on alumina ($Al_2O_3$), platinum (Pt), aluminium nitride (AlN) and 0.65PMN–0.35PT substrates. The films were then characterized using scanning electron microscopy, X-ray diffraction and dielectric constant measurements. The X-ray analysis did not detect the presence of any undesirable pyrochlore phase, and the differences in the phase compositions were determined with a Rietveld refinement. The variations of the cell parameters vs. the temperature for the monoclinic and tetragonal phases were calculated. It was demonstrated that under similar processing conditions the microstructures, phase compositions and dielectric properties strongly depended on the stress in the thick films due to the different temperature expansion coefficients of the thick films and the substrates. The 0.65PMN–0.35PT thick films under compressive stresses (for the case of the $Al_2O_3$ and Pt substrates) exhibited a tetragonal phase in addition to the monoclinic one. The films were sintered to a high density and with a coarse microstructure. These microstructures favour a high dielectric constant. In contrast, for the films under a tensile stress, like the films on AlN substrates, the films were sintered to a lower density and the microstructure consisted of smaller grains. The X-ray analysis showed mainly a monoclinic phase, while the tetragonal phase was not detected. These results indicate the importance of the stresses in 0.65PMN–0.35PT thick films and their influence on the structural and electrical characteristics of the films.

© 2010 Elsevier Ltd. All rights reserved.

*Keywords:* 0.65PMN–0.35PT; Films; Residual stress; X-ray methods; Electrical properties

## 1. Introduction

In recent years the fabrication of ceramic ferroelectric and piezoelectric thick and thin films has been extensively studied, with a particular emphasis on the impact with respect to micro and nano devices. These films are known to be clamped by the substrates and for this reason their properties, which are stress sensitive, differ from those of bulk ceramics.[1–6] These differences between the characteristics of the bulk materials and the films are still a subject of much interest.

Ferroelectric and piezoelectric films are mostly based on lead oxide compounds, mainly $Pb(Zr,Ti)O_3$ (PZT) solid solutions. Compositions of the so-called morphotropic phase boundary (MPB) region, where the properties are the highest, in PZT for

both bulk ceramics and thin films were studied theoretically and experimentally.[7–14] A great deal of effort was made to understand the differences in the behaviour between bulk PZT and thin films.[2–4] However, although films with thicknesses below 1 μm were frequently investigated, thick films with thicknesses of a few tens of microns have received much less attention.

An alternative to PZT is the relaxor-based systems whose prototype is the $(1 − x)Pb(Mg_{1/3}Nb_{2/3})O_3$–$xPbTiO_3$ (PMN–PT) material. PMN–PT with a MPB composition around $x \approx 0.35$ (0.65PMN–0.35PT) has always been the subject of intense research, because it exhibits giant piezoelectric properties and a high dielectric constant.[15–18] It is worth mentioning that the strong piezoelectric properties of these solid solutions are related to the "polarization rotation" between the adjacent rhombohedral and tetragonal phases through one (or more) intermediate phase(s) of low-symmetry, i.e., a monoclinic (orthorhombic or triclinic) phase.[19] As a consequence, the observation of a low-symmetry phase, typically a monoclinic one, may sug-

* Corresponding author. Tel.: +386 1 477 3414; fax: +386 1 477 38 87.
*E-mail address:* hana.ursic@ijs.si (H. Uršič).

Table 1
The processing conditions and dielectric constants $\varepsilon$ of 0.65PMN–0.35 PT ceramics obtained by different authors.

| Literature | Processing conditions | $\varepsilon$ (frequency) |
|---|---|---|
| Koo and Cheong[15] | The columbite method $T_{firing}$ 1200–1250 °C, 5 h, poled sample | 6350 (1 kHz) |
| Alguero et al.[16] | The mechanochemical method $T_{firing}$ 1200 °C | ~2000 (2 kHz) |
| Kelly et al.[17] | The columbite method $T_{firing}$ 1250 °C, 1.5 h | 5200 (1 kHz) |
| Singh and Pandey[18] | The columbite method $T_{firing}$ 1260 °C, 2 h | 3000 (1 kHz) |
| Leite et al.[25] | The columbite method hot-pressed $T_{firing}$ 1150 °C, 5 h | ~4000 (1 kHz) |
| Xia et al.[26] | $T_{firing}$ 1200 °C, 2 h | 4000 (1 kHz) |

gest strong electromechanical responses. In 2001, Singh and Pandey reported that the structure of 0.66PMN–0.34PT can be described by a monoclinic phase with the space group Pm, while 0.65PMN–0.35PT has a tetragonal structure with the space group P4mm.[20] Nevertheless, one year later, in 2002, a monoclinic phase with the space group Pm for the 0.65PMN–0.35PT composition at room temperature was also reported.[21] The temperature dependence of the Pm monoclinic phase was studied for compositions between 0.7PMN–0.3PT and 0.61PMN–0.39PT, and the stability region of the monoclinic phase at 20 K was determined, i.e., $x = 0.31$–0.37.[22] Later results[16,18,23,24] showed the coexistence of the monoclinic Pm and the tetragonal P4mm phases at room temperature for non-poled 0.65PMN–0.35PT ceramics. For example, Alguero et al.[23] reported that the ratio of the tetragonal-to-monoclinic phases is higher for larger grains. The ceramics with 4-μm grains contain 11% of the tetragonal phase, while the ceramics with 0.15-μm grains contain 5% of tetragonal phase. In fact, many published results about the structure–composition relationship are puzzling, confusing and even contradictory, which highlights the key role played by the synthesis process.

Moreover, for 0.65PMN–0.35PT ceramics, different values of the dielectric constant $\varepsilon$ measured at ~1 kHz were reported, i.e., from 2000 to 6350.[15,17,18,23,25,26] Some values, together with processing conditions, are summarized in Table 1.

Thick films with the 0.65PMN–0.35PT composition were prepared on both $Al_2O_3$ and Si substrates.[5,6,27,28] When fired at around 950 °C, the values of $\varepsilon$ for the thick films on $Al_2O_3$ substrates were found to vary from 3600 to 4100 when measured at 1 kHz,[6,27,28] while for 0.65PMN–0.35PT thick films on Si substrates the values were around 2000.[27]

The aim of this study was to investigate the influence of the substrates on the properties of 0.65PMN–0.35PT thick films. Here, we report on the structure, microstructure and dielectric properties obtained from thick films deposited on alumina ($Al_2O_3$), platinum (Pt), aluminium nitride (AlN) and 0.65PMN–0.35PT substrates. These substrates were chosen because of their different temperature coefficients of expansion (TEC). Two of the substrates have higher TECs in comparison
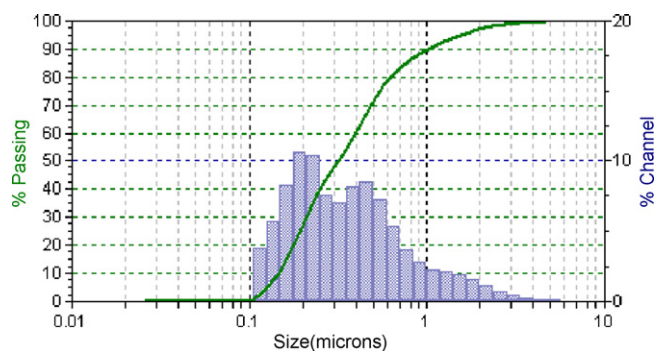


Fig. 1. The particle-size distribution of the 0.65PMN–0.35PT powder. The line is the cumulative curve.

with the TEC of the 0.65PMN–0.35PT films, i.e., the polycrystalline alumina substrates and the metal platinum substrates, another substrate had a lower TEC, i.e., the AlN, and the last type of substrate was made from a material with the same composition as the films and therefore had the same TEC, i.e., 0.65PMN–0.35PT. To the best of the authors' knowledge, no systematic studies on the influence of the stresses resulting from the difference in the TECs between the substrates and PMN–PT thick films were published in the open literature. It was expected that even for thick films with thicknesses of a few tens of μm, the nature of the substrates could affect the structure and microstructure and thus the dielectric properties. These findings will be of fundamental interest as well as being important for the future integration of these thick films into electronic devices.

## 2. Experimental

As the starting compounds for the synthesis of the 0.65PMN–0.35PT material, PbO (99.9%, Aldrich), MgO (98%, Aldrich), $TiO_2$ (99.8%, Alfa Aesar) and $Nb_2O_5$ (99.9%, Aldrich) were used. A mixture of these oxides in the molar ratio corresponding to a stoichiometry of $0.65Pb(Mg_{1/3}Nb_{2/3})O_3$–$0.35PbTiO_3$ (0.65PMN–0.35PT) with an excess of 2 mol% PbO was high-energy milled in a planetary mill (Retsch, Model PM 400). An excess amount of PbO was added for two reasons: to advance the sintering with the formation of a liquid phase rich in PbO and to replace the PbO lost from the PMN–PT during the sintering. After the mechanochemical synthesis, the powder was milled in an attritor mill at 800 rpm for 4 h in isopropanol, and then dried and sieved using a polyethylene sieve with a 0.5-mm opening. The powder was than heated at 700 °C for 1 h.

The size of the particles in the starting 0.65PMN–0.35PT powder prepared by the mechanochemical synthesis was determined by a light-scattering technique using a Microtrac S3500 Series Particle Size Analyzer. All the measurements were performed in isopropanol. The results were derived from the area particle-size distribution, which is shown in Fig. 1. The cumulative curve is also shown. The spread of the particle dimensions is between 0.1 μm and around 5 μm, with 90% of the particles having a size smaller than 1 μm. The particle-size distribution is narrow; median particle-size $d_{50}$ is equal to 0.32 μm.
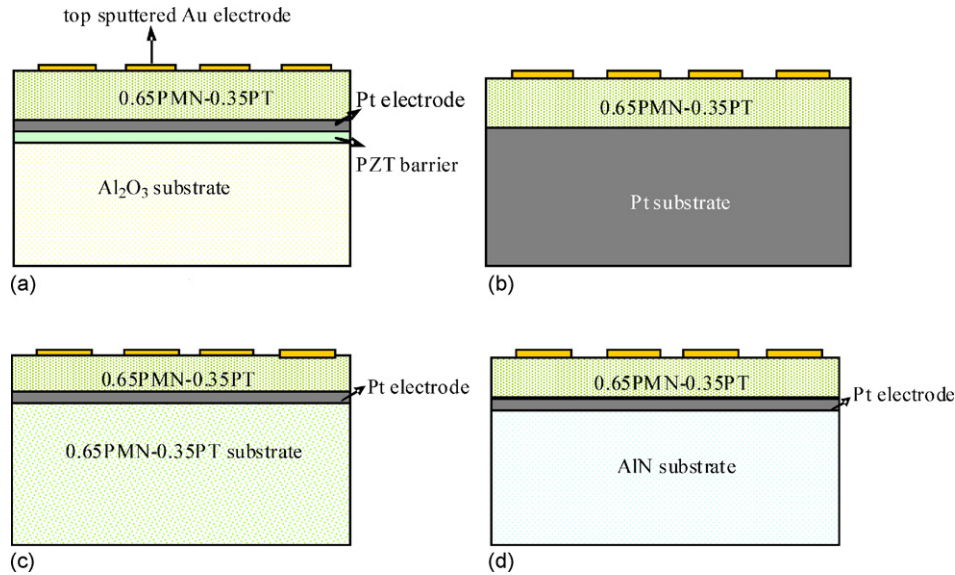
Fig. 2. Scheme of cross-sections of the 0.65PMN–0.35PT films on (a) Al$_2$O$_3$, (b) Pt, (c) 0.65PMN–0.35PT and (d) AlN substrates.

The 0.65PMN–0.35PT thick-film paste was prepared from a mixture of a powder with this composition and an organic vehicle consisting of alpha-terpineol 2-2-butoxy-ethoxy-ethyl acetate and ethyl cellulose, in the ratio 60:25:15.

The 2-mm-thick platinum substrates were obtained from Zlatarna Celje (Pt 9 9 9). The 3-mm-thick alumina substrates were prepared by slip casting from Alcoa A-16 and sintering at 1600 °C for 4 h. The 1.5-mm-thick 0.65PMN–0.35PT substrates were prepared by pressing this powder isostatically at 300 MPa and then sintering them in a covered alumina vessel in 0.65PMN–0.35PT packing powder at 1200 °C for 2 h. The heating rate was 3 °C/min. The 0.64-mm-thick aluminium nitride substrates were obtained from CeramTec (AlN AlunitR).

PbZr$_{0.53}$Ti$_{0.47}$O$_3$ (PZT-0.53/0.47) powder with an excess of 6 mol% PbO was used as a barrier between the alumina substrates and the active structure to prevent interactions.[29–32] It was prepared by mixed-oxide synthesis at 900 °C for 1 h from high-purity PbO 99.9% (Aldrich), ZrO$_2$ 99% (Tosoh), and TiO$_2$ 99% (Alfa Aesar). The thick-film paste was prepared from pre-reacted PZT-0.53/0.47 powder and the organic vehicle. After printing the PZT-0.53/0.47 layer on the alumina substrate, samples were heated at 500 °C for 1 h to evaporate the organic compounds from the PZT-0.53/0.47 paste and then sintered at 1100 °C for 2 h. The thickness of the PZT-0.53/0.47 barrier after firing was around 15 μm.

A Pt paste (Ferro 6412), which was used as a bottom electrode, was printed and fired at 1200 °C for 1 h on 0.65PMN–0.35PT and AlN substrates and on a PZT-0.53/0.47 layer in the case of the Al$_2$O$_3$ substrate. The thickness of the bottom Pt electrode was around 10 μm. On the Pt substrate, a Pt bottom electrode was not printed as the conductive Pt substrate itself was used as the electrode.

The 0.65PMN–0.35PT paste was printed twice, with intermediate drying at 150 °C after each printing step. The samples were then heated for 1 h at 500 °C to burn out the organic vehicle from the paste, then sintered at 950 °C for 2 h in PbZrO$_3$ packing powder with an excess of 2 mol% PbO and then cooled down with a rate of 3 °C/min. Fig. 2 shows schematically the cross-sections of each of the 0.65PMN–0.35PT films on the Al$_2$O$_3$, Pt, 0.65PMN–0.35PT and AlN substrates.

The thickness of 0.65PMN–0.35PT films with the same number of printed layers, i.e., two layers, prepared at the same firing and cooling conditions differs with the choice of the substrates. For films on Al$_2$O$_3$, Pt, 0.65PMN–0.35PT and AlN substrates the thicknesses were 21, 20, 26 and 34 μm, respectively. Films on 0.65PMN–0.35PT and AlN substrates are thicker than the films on Al$_2$O$_3$ and Pt substrates due to the lower sintering density of the films on these substrates.

For a comparison with the thick-film samples, which were fired at 950 °C for 2 h, bulk ceramics were prepared by using the same powder as the films and fired under the same conditions, i.e., in a covered alumina vessel in 0.65PMN–0.35PT packing powder at 950 °C for 2 h. The heating rate was 3 °C/min. Before firing the pellets were isostatically pressed at 300 MPa. After sintering, the pellets were cut, polished and annealed at 600 °C for 1 h with a cooling rate of 1 °C/min to release the stresses induced by the polishing. After cutting the pellets had a diameter of 6 mm and a thickness of 1 mm.

The fired films were analyzed by X-ray diffraction using Cu K$_{\alpha1}$ radiation ($\lambda = 1.54051$ Å) and a Philips PW 1710 X-ray diffractometer. The X-ray diffraction patterns were measured from $2\theta = 10°$ to $2\theta = 70°$ using a step of 0.033° and a time per step of 1 s. The phase composition was determined with a Rietveld analysis of these patterns, using the software Jana2006.[33] We used the starting unit-cell parameters and the atomic positions from a former Rietveld study made by Singh and Pandey.[18] The atomic positions proposed by Singh et al. were not modified. The background, the shift, the unit-cell parameters, the profile parameters, the phase ratio and the preferential orientation were refined to obtain the lowest reliability factors, corresponding to the best agreement between the experimental and calculated diffraction patterns. This refinement allowed us to determine the amount of both expected phases, i.e., the monoclinic Pm and the tetragonal P4mm.

In order to determine the structural phase transitions, a two-axis diffractometer in Bragg–Brentano geometry with Cu K$_\beta$ radiation ($\lambda = 1.3922$ Å) was measured from −173 to 127 °C using a temperature interval of 20 °C and from 127 to 200 °C using an interval of 10 °C. As such experiments are time consuming, selected reflections, corresponding to the pseudocubic (2 0 0), (2 2 0) and (2 2 2) Bragg peaks, were recorded. The corresponding measured intervals are as follows: from $2\theta = 39.75°$ to $2\theta = 41.25°$ (2 0 0), from $2\theta = 58.00°$ to $2\theta = 59.5°$ (2 2 0) and from $2\theta = 73.00°$ to $2\theta = 74.3°$ (2 2 2), using a step of 0.01°. These three major reflections were indeed sufficient to see the changing of the parameters and the symmetry in the 0.65PMN–0.35PT with increasing temperature.

The thermal expansion coefficient (TEC) of the bulk 0.65PMN–0.35PT was determined using a dilatometer (Netzsch DIL 402EP) on samples of cylinders with the diameter $2r = 7.5$ mm and the length $d = 27$ mm. The measurements of the sample expansion vs. temperature were made from 30 to 490 °C with temperature intervals of 10 °C.

For the electrical measurements, round-top electrodes with a 3-mm diameter were deposited by sputtering. For the bulk ceramics, gold electrodes with a surface of 19.6 mm$^2$ were sputtered on both sides. The dielectric constants were measured with a HP 4284 A Precision LCR impedance meter in the temperature range −150 to 300 °C at 100 kHz. The measurements of dielectric constant versus temperature were made in two steps: at a low temperature from −150 to 70 °C, in a vacuum chamber, and from 70 to 300 °C, in a furnace in the air. The dielectric data were collected during cooling.

A JEOL JSM 5800 scanning electron microscope (SEM) equipped with an energy-dispersive X-ray analyser (EDS) was used for the overall microstructural analysis. Prior to the SEM analysis, the samples were sputtered with a carbon film to provide electrical conductivity and to avoid charging. For the micrograph of the 0.65PMN−0.35PT film on the AlN substrate and the bulk ceramics fired at 950 °C the FE-SEM, Supra 35 VP, Carl Zeiss was used at 5 kV. For the grain size estimation the polished cross-sections of the samples were thermally etched at 900 °C for 20 min and the SEM micrographs were made. Feret's
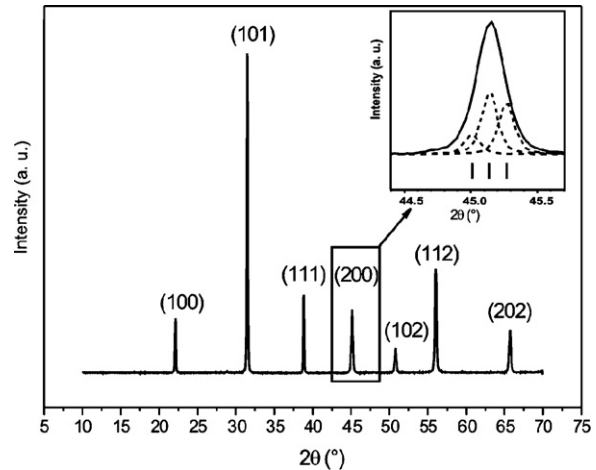


Fig. 3. The X-ray diffraction diagram of 0.65PMN–0.35PT ceramics fired at 950 °C. Inset shows the family of (2 0 0) peaks. The refined peak positions (0 0 2), (2 0 0), (0 2 0) of the monoclinic Pm phase are marked.

diameter ($d_F$) was used to get a median value $d_{50}$ of the grain size using microscopic measurements.

## 3. Results

### 3.1. Structure and phase composition

#### 3.1.1. Bulk 0.65PMN–0.35PT ceramics fired at 950 °C

As already mentioned, for a comparison with the thick films of nominal composition 0.65PMN–0.35PT, an X-ray diffraction pattern of a bulk ceramic fired at 950 °C was recorded and is shown in Fig. 3. At first glance, the Bragg peaks appear single, but abnormally broad. Different phases were considered, including cubic, tetragonal, monoclinic, etc. symmetries and also mixtures of different phases. The best agreement factor and matching between the observed and calculated profiles were obtained with only a monoclinic Pm phase and the unit-cell parameters: $a = 4.0160(1)$ Å, $b = 4.0057(1)$ Å, $c = 4.0271(2)$ Å and $\beta = 90.091(3)°$. The inset in Fig. 3 shows a pseudo-cubic
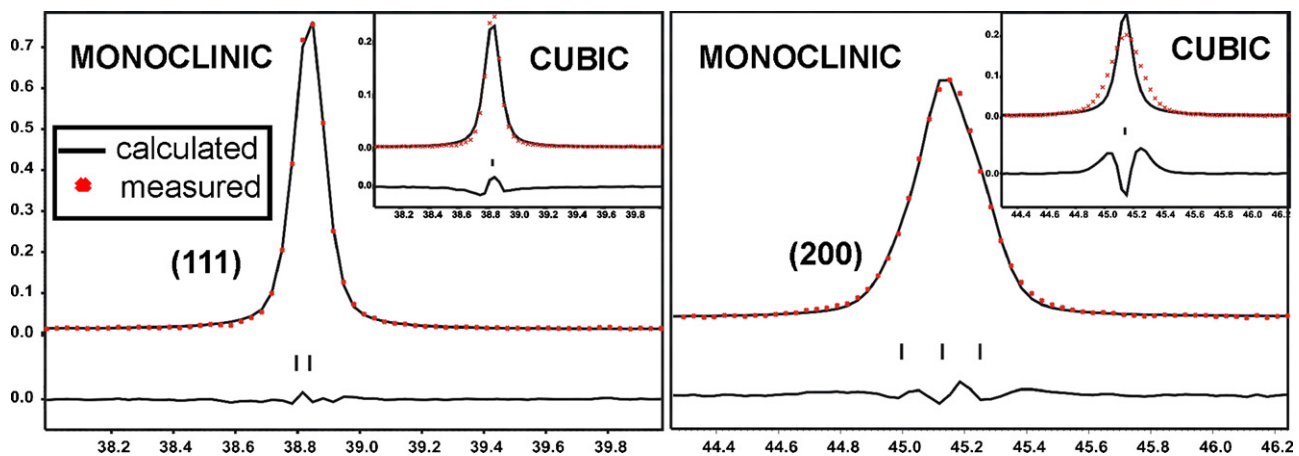


Fig. 4. Two regions (a) from $2\theta = 38°$ to $2\theta = 40°$ and (b) from $2\theta = 44.2°$ to $2\theta = 46.4°$ of the measured X-ray diffraction for the ceramics and the profile matching for the monoclinic Pm phase. Insets: the profile matching for the cubic Pm–3m phase is also added for comparison.

{2 0 0}-like Bragg peak with the monoclinic Pm peak positions of (0 0 2), (2 0 0) and (0 2 0) indicated.

For comparison, in Fig. 4 we plotted both the {1 1 1} (Fig. 4a) and {2 0 0} (Fig. 4b) Bragg reflections obtained with the final monoclinic Pm phase, with the inset showing the refinement result obtained by considering a cubic Pm–3m phase. It is obvious that while the Bragg peaks appear single, the diffraction pattern does not correspond to a cubic phase, but rather to a monoclinic one. We tried a mixture of the monoclinic Pm phase with the tetragonal P4mm one, but no improvement in the refinement was obtained. Therefore, the prepared bulk ceramics at 950 °C are described by a monoclinic phase, while a small amount (not detected in our X-ray data) of tetragonal phase cannot be completely excluded.

### 3.1.2. 0.65PMN–0.35PT thick films at room temperature

The X-ray diffraction patterns were measured for the 0.65PMN–0.35PT thick films on the $Al_2O_3$, Pt, 0.65PMN–0.35PT and AlN substrates. In Fig. 5 the indexed peaks of the perovskite phase are shown for the films on alumina substrates.

The complete diffraction patterns for all the synthesized thick films are shown in Fig. 6. First of all, no extra diffraction peaks that might correspond to pyrochlore or PbO phases were detected, stressing the high process efficiency. It is also worth noting that whereas the Bragg peaks appear single in the case of the 0.65PMN–0.35PT (Fig. 6c) and AlN (Fig. 6d) substrates, some splitting is clearly observed for the alumina
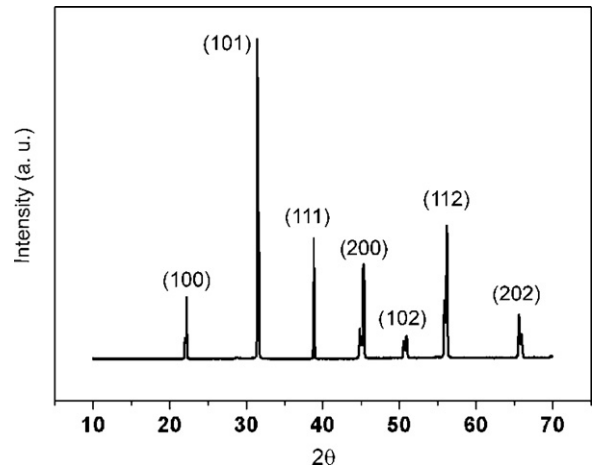


Fig. 5. The X-ray diagram of the 0.65PMN–0.35PT film on the alumina substrate. The families of planes are given in brackets.

(Fig. 6a) and Pt (Fig. 6b) substrates. This result is very surprising as the thick films were synthesized with the same powder, at the same temperature, for the same time and with the same cooling regime.

For the sake of clarity, Fig. 7 focuses on the region of the diffraction pattern corresponding to the cubic-like (2 0 0) Bragg peak. It is clear that for describing the peaks for a film on the $Al_2O_3$ and Pt substrates, one must consider the coexistence of phases. Rietveld refinements allowed us to show that for these films, a mixture of the tetragonal P4mm and
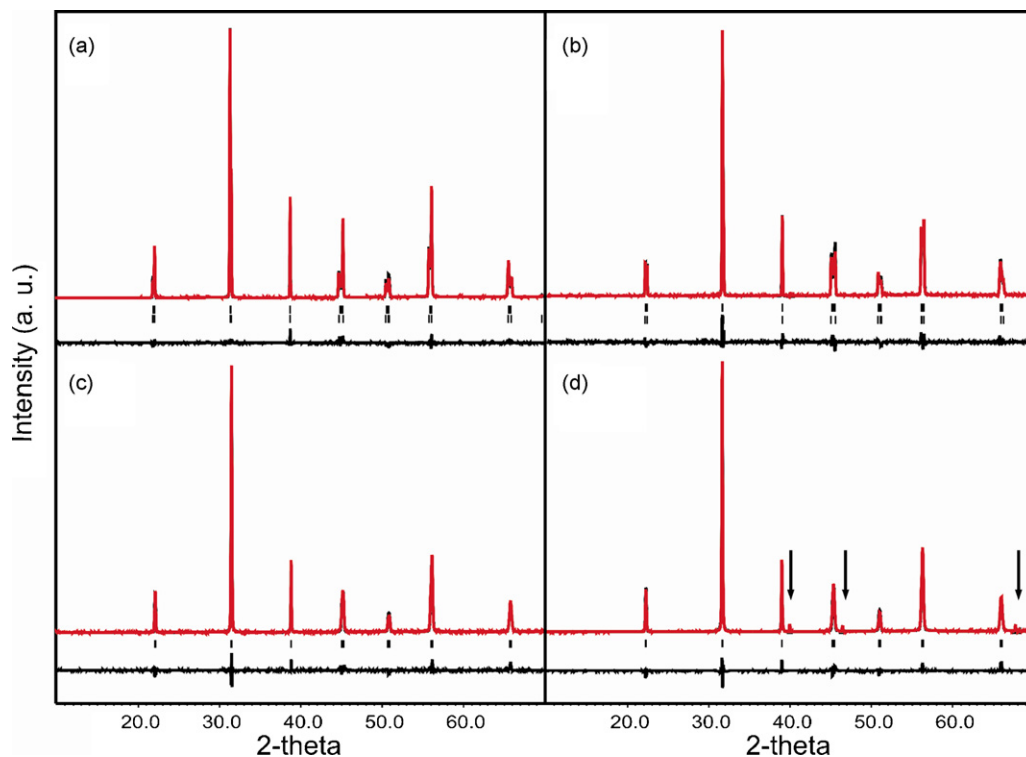


Fig. 6. Final observed (red), calculated (black) and difference curves of the X-ray diffraction Rietveld refinement for films deposited on (a) $Al_2O_3$, (b) Pt, (c) 0.65PMN–0.35PT and (d) AlN. The top marks correspond to the tetragonal phase and the bottom ones to the monoclinic. The positions corresponding to the Pt electrode (arrows) were excluded from the refinement. (For interpretation of the references to color in this figure legend, the reader is referred to the web version of the article.)
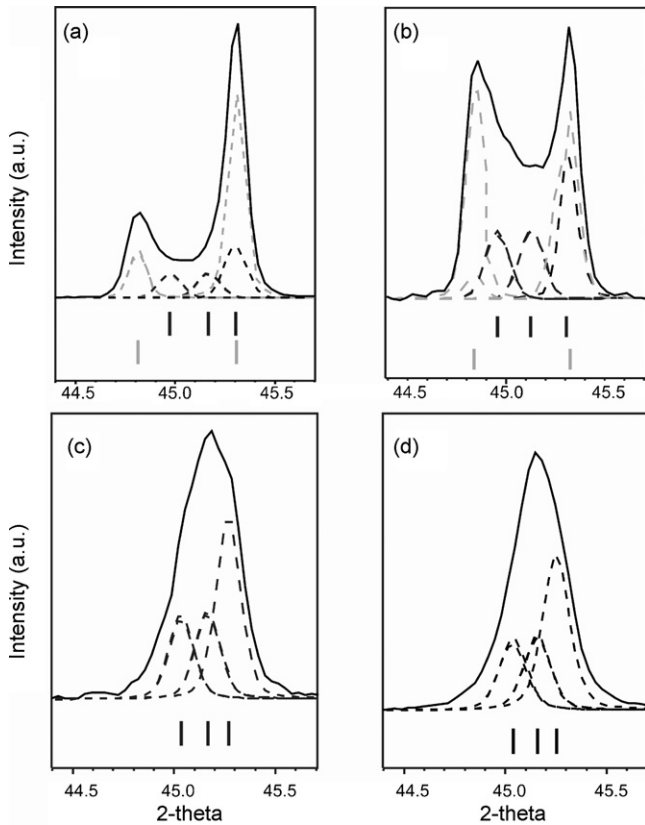
Fig. 7. The X-ray diffraction diagrams of 0.65PMN–0.35PT thick films on (a) Al$_2$O$_3$, (b) Pt, (c) 0.65PMN–0.35PT and (d) AlN substrates in the range from $2\theta = 44.4°$ to $2\theta = 45.7°$. The refined peak positions of the (0 0 2), (2 0 0) tetragonal (grey) and the (0 0 2), (2 0 0), (0 2 0) monoclinic (black) phases are marked.

Table 2
Phase ratio, reliability factors $R$, for the monoclinic Pm ($R_M$) and tetragonal P4mm ($R_T$) phases and goodness of fit (Gof), from the Rietveld analysis of the X-ray data measured at room temperature.

| Substrate | Phase ratio in percentage (%) (monoclinic Pm: tetragonal P4mm) | $R_M$ | $R_T$ | Gof |
|---|---|---|---|---|
| Al$_2$O$_3$ | 42:58 | 5.58 | 5.85 | 1.75 |
| Pt | 81:19 | 3.68 | 4.18 | 1.19 |
| 0.65PMN–0.35PT | 100:0 | 4.31 | – | 1.10 |
| AlN | 100:0 | 5.49 | – | 1.89 |

### 3.1.3. Temperature dependence of the phase composition

To understand and clarify the coexistence of the monoclinic and tetragonal phases, the X-ray diffraction patterns of the 0.65PMN–0.35PT films were measured at different temperatures, i.e., from −173 to 200 °C. It is first worth recalling that the bulk 0.65PMN–0.35PT powder exhibits two phase transitions: one from the cubic to the tetragonal phase at around 170 °C[22,26,34] and another from the tetragonal to the monoclinic phase above room temperature, around 50 °C.[22,26,34,35] Note that this last phase transition is of the first order, with a coexistence of monoclinic and tetragonal phase over a wide temperature range (see X-ray data below). The X-ray diffraction patterns for the cubic-like (2 0 0) peak for the film deposited on the alumina substrate at different temperatures are shown in Fig. 8.

At high temperatures of 187 and 200 °C, the diffraction pattern with single Bragg peaks is described by a cubic Pm–3m phase. At 177 °C, a new peak on the left-hand side (at a lower angle) of the main Bragg peak appears, attesting to the occurrence of the tetragonal phase. This critical temperature is slightly higher than that expected for the bulk 0.65PMN–0.35PT. This discrepancy may arise due to stress, similar to the case of thin BaTiO$_3$ films, as reported in Ref.[36] The peak splitting is well understood by considering a tetragonal phase down to 107 °C,

the monoclinic Pm phases is needed to describe the whole diffraction pattern, as demonstrated in Fig. 7. Indeed, the (0 0 2) and (2 0 0) tetragonal peaks and the (0 0 2), (2 0 0) and (0 2 0) monoclinic peaks can be clearly seen. Thanks to the Rietveld refinement, it is possible to extract the amount of each phase. As a result, 42% of the Pm and 58% of the P4mm phase was determined in the 0.65PMN–0.35PT thick films on alumina substrates at room temperature, and for the films on Pt substrates, the amounts of monoclinic Pm and tetragonal P4mm phases were 81% and 19%, respectively. Taking into account the (0 0 1) partial preferential orientation for the tetragonal phase improved the quality of the refinement. The ratio of the intensities $I_{(0 0 1)}/(I_{(1 0 0)} + I_{(0 1 0)} + I_{(0 0 1)})$ for these films was 0.66, whereas for the non-oriented films it was 0.33. In contrast, for the films on the 0.65PMN–0.35PT and AlN substrates, no tetragonal phase was evidenced and the monoclinic Pm phase alone was determined from the X-ray diffraction.

In Table 2, the calculated phase ratio (monoclinic-to-tetragonal) in a percentage, the reliability factors $R$ for the monoclinic and tetragonal phases, and the goodness of fit for the profile, Gof, are collected for the 0.65PMN–0.35PT thick films on the Al$_2$O$_3$, Pt, 0.65PMN–0.35PT and AlN substrates. The values of the reliability factors and the goodness of fit are acceptable, taking into account the fixed atomic positions.
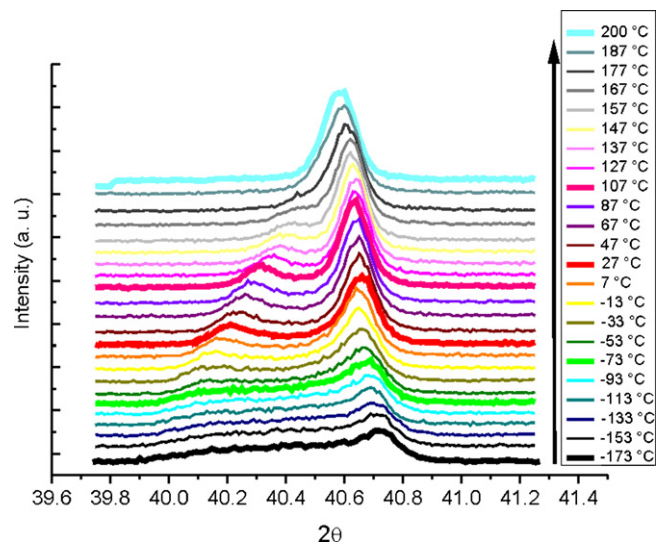


Fig. 8. The X-ray diffraction diagram of 0.65PMN–0.35PT films on alumina substrates measured at different temperatures. The black arrow indicates the increase of the temperatures.
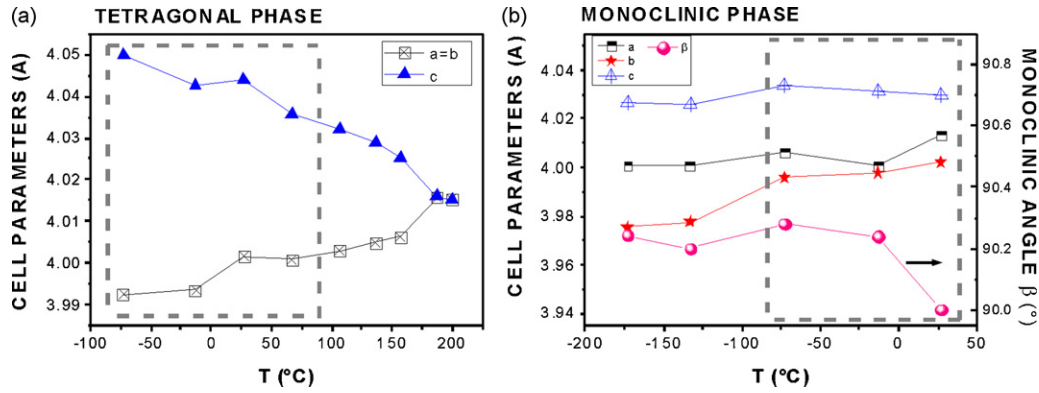
Fig. 9. Variations of cell parameters with temperature for (a) the tetragonal P4mm and (b) the monoclinic Pm phases of the 0.65PMN–0.35PT films on alumina substrates. The dashed rectangle shows the area of the coexistence of the tetragonal P4mm and monoclinic Pm phases. The line between the measured values is just a guide to the eye.

but below this temperature an additional intensity is observed in between the two tetragonal Bragg peaks. This is an indication of the appearance of the monoclinic phase. At 107 °C the phase is tetragonal, however below 107 °C the coexistence of monoclinic and tetragonal appears. At 87 °C the percentage of monoclinic phase is very small, but it is increasing with decreasing temperature. At room temperature, i.e., 27 °C the phase ratio is 42% of monoclinic Pm phase and 58% of tetragonal P4mm phase, as explained in the previous section. When the temperature decreases below the room temperature, i.e., 27 °C, the amount of tetragonal phase decreases. The weak distortion of tetragonal phase can still be present at −53 and −73 °C and cannot be completely excluded. Below the −73 °C the phase is a pure monoclinic Pm. Fig. 9 shows the variations of the unit-cell parameters with temperature for both the monoclinic Pm and the tetragonal P4mm phases.

With decreasing temperature the tetragonal $a$-parameter decreases, while the $c$-parameter increases, describing the enhancement of the tetragonal strain, which reaches a value of ∼1.4% at −73 °C. The monoclinic unit-cell parameters decrease very weakly with the decreasing temperature. The beta monoclinic angle is relatively stable at 90.24° (±0.04°) until 27 °C, where it drops to a value close to 90°. In Fig. 9, the dashed rectangle shows the area of coexistence of the tetragonal P4mm and the monoclinic Pm phases. Between 67 and 87 °C, a small amount of monoclinic phase is detected, but due to the very weak intensity of its reflections, the positions cannot be refined.

Fig. 10 shows the X-ray diagrams of the (2 0 0) cubic-like peak measured at different temperatures for the film on a Pt substrate. The same tendencies as with the film deposited on the Al₂O₃ substrate are observed. At a low temperature, the monoclinic Pm is found for the 0.65PMN–0.35PT films on Pt substrates. The tetragonal phase is detected above −33 °C, with a tetragonal strain of ∼1.1%. At room temperature, i.e., 27 °C, as was already mentioned, the phase ratio is 81% of the monoclinic Pm phase and 19% of the tetragonal P4mm phase. Above 177 °C, the cubic Pm–3m phase appears. In Fig. 11, the temperature dependence of the cell parameters for the monoclinic Pm and the tetragonal P4mm phases are shown.

Like with the films on Al₂O₃ substrate, the monoclinic unit-cell parameters change very slowly with temperature. The

monoclinic beta angle is relatively stable at 90.27° (±0.03°) until −13 °C, after which it starts to decrease to reach a value close to 90° at 27 °C. In Fig. 11 the dashed rectangle shows the area of the coexistence of the tetragonal P4mm and the monoclinic Pm phases.

The situation for the 0.65PMN–0.35PT films on the 0.65PMN–0.35PT and AlN substrates is different, as both show the same tendency, with a monoclinic phase existing alone at 27 °C. The temperature dependence of the (2 0 0) cubic-like diffraction peak is shown for films on the 0.65PMN–0.35PT substrate (see Fig. 12).

From −173 up to 177 °C, the structure is described by just a monoclinic phase for films on the 0.65PMN–0.35PT and AlN substrates, and no tetragonal phase was detected up to the Curie temperature. Above 177 °C, the phase is cubic Pm–3m. Nevertheless, the high-temperature diffraction patterns are so complex with asymmetric broadening that it is not possible to exclude the occurrence of a tetragonal phase below 177 °C. Fig. 13 shows the temperature evolution of the unit-cell parameters for the monoclinic Pm phase to the cubic phase. The features, i.e., the lattice
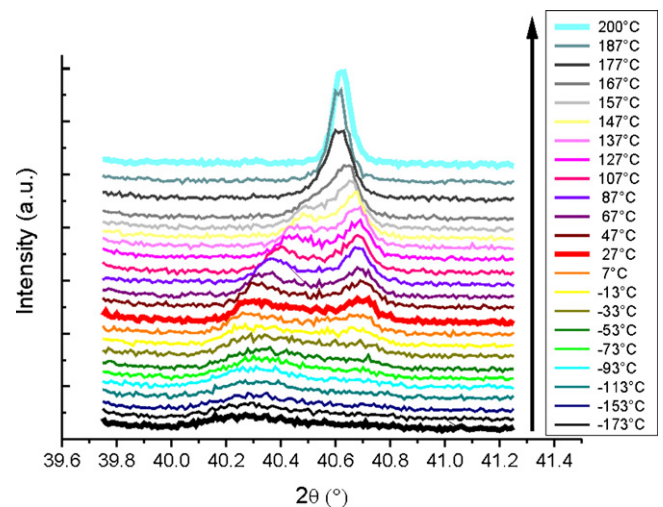


Fig. 10. The X-ray diffraction diagram of 0.65PMN–0.35PT films on Pt substrates measured at different temperatures. The black arrow indicates an increase of the temperature.
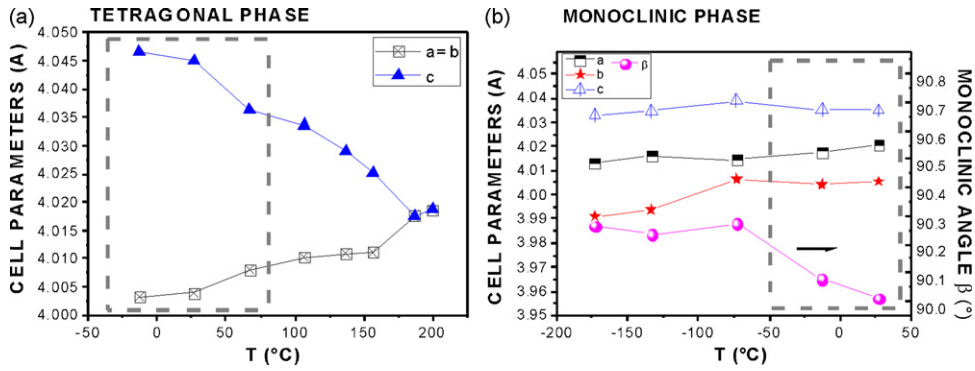
Fig. 11. Variation of the cell parameters with temperature for (a) the tetragonal P4mm and (b) the monoclinic Pm phases of 0.65PMN–0.35PT films on Pt substrates. The dashed rectangle shows the area of the coexistence of the tetragonal P4mm and the monoclinic Pm phases. The line between the measured values is just a guide to the eye.

parameters and the beta angle, are also similar for the Pt substrate (Fig. 11). It is worth noting that the beta angle shows two regions. Above $27\,°C$, the value of the angle is almost constant with a typical value of $90.05°$, which is very close to $90°$. Below $27\,°C$, the beta angle increases continuously, reaching a value of $90.28°$ at $-173\,°C$. Such behaviour might reflect the occurrence of another phase. In other words, it is possible that a tetragonal phase also appears in these films, but the tetragonal distortion is very weak, which makes it difficult to distinguish between a monoclinic and a tetragonal phase in the refinement.

### 3.2. Microstructures of the thick films

Let us now turn our attention to the microstructure. The SEM micrograph of the surface of a sample screen-printed, dried and heated at $500\,°C$ for $1\,h$ (to burn out the organic vehicle) of a 0.65PMN–0.35PT thick film is shown in Fig. 14. As expected from the particle-size distribution (see Fig. 1), the film shows 0.65PMN–0.35PT grains with mainly sub-micron dimensions.

The representative SEM micrographs of the 0.65PMN–0.35PT film surfaces, fired at $950\,°C$ for $2\,h$, on $Al_2O_3$, Pt, 0.65PMN–0.35PT and AlN substrates are shown in Fig. 15a–d, respectively. All the samples exhibit porosity. The films on the $Al_2O_3$ and Pt substrates are sintered to a high density and have significant grain growth. The median grain sizes are $1.7 \pm 0.6\,\mu m$ for the films on the $Al_2O_3$ substrate and $1.2 \pm 0.3\,\mu m$ for the films on the Pt substrate.
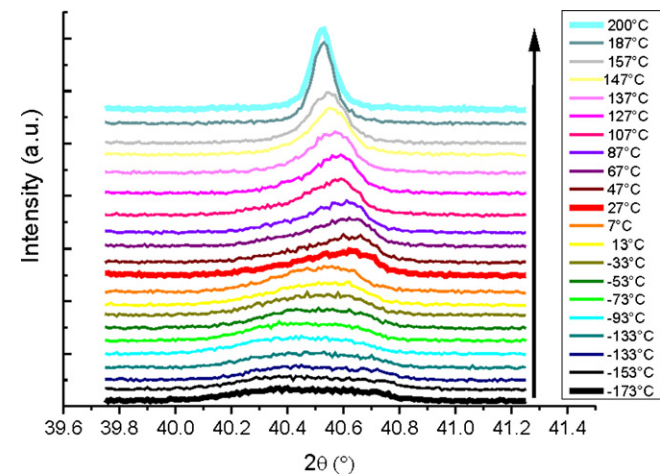


Fig. 12. The X-ray diffraction diagram of 0.65PMN–0.35PT films on 0.65PMN–0.35PT substrates measured at different temperatures. The black arrow indicates the increase of the temperature.
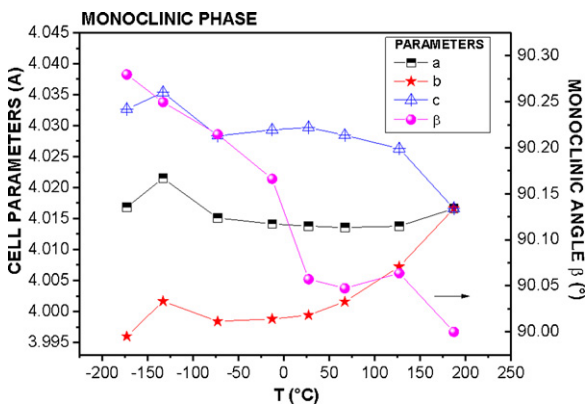


Fig. 13. Variation of the cell parameters with temperature for the monoclinic Pm phase of 0.65PMN–0.35PT films on 0.65PMN–0.35PT substrates. The line between the measured values is just a guide to the eye.
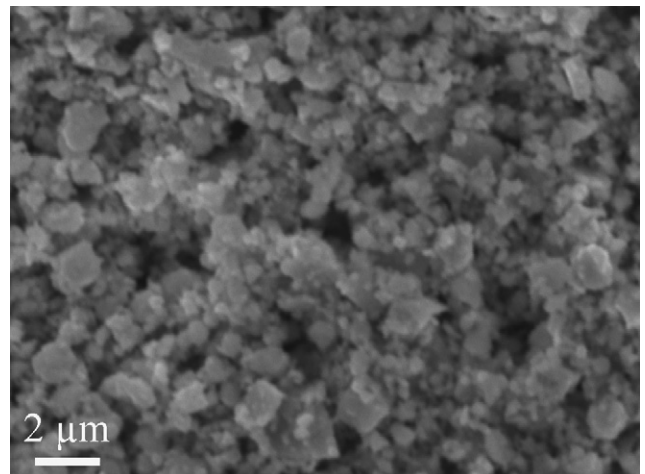


Fig. 14. The microstructure of the surface of a 0.65PMN–0.35PT thick film that was screen-printed, dried and heated to $500\,°C$.
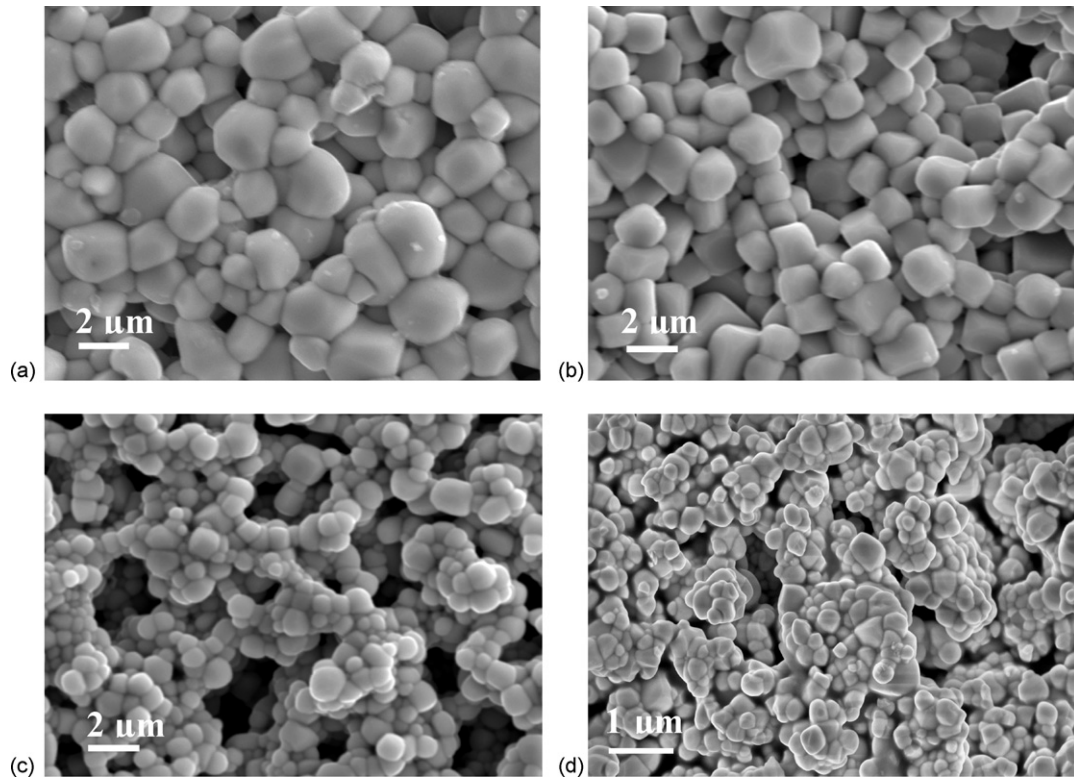
Fig. 15. The SEM micrographs of the surface of 0.65PMN–0.35PT thick films on (a) $Al_2O_3$, (b) Pt, (c) 0.65PMN–0.35PT and (d) FE-SEM micrograph of the surface of 0.65PMN–0.35PT thick films on AlN substrates.

The grains are a few times larger than the grains of the un-fired 0.65PMN–0.35PT powder. In contrast, the microstructures of the films on the 0.65PMN–0.35PT and AlN substrates are more porous and consist of small grains with dimensions $0.5 \pm 0.2\,\mu m$ and $0.3 \pm 0.1\,\mu m$, respectively. However, grain boundaries can be observed, attesting to the sintering effect.

Fig. 16 shows the fracture microstructure of the bulk 0.65PMN–0.35PT ceramics fired at 950 °C with a grain size and porosity similar to those of the films deposited on the AlN substrate. The grains have mainly sub-micron dimensions. The determined porosity is around 71%, based on the measured density ($\rho = 5.80$ g/cm$^3$) and the theoretical density calculated from
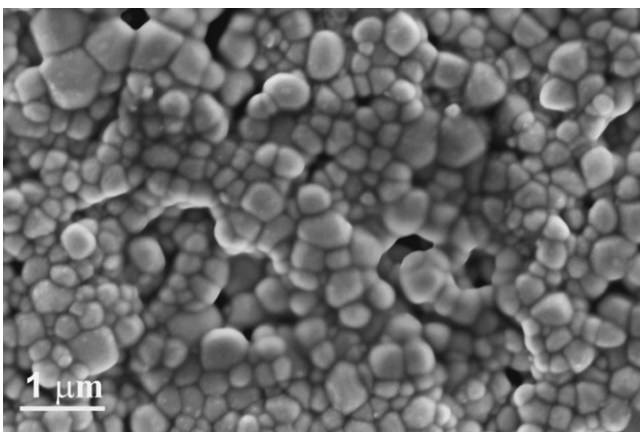


Fig. 16. The FE-SEM micrographs of fracture for bulk 0.65PMN–0.35PT ceramics fired at 950 °C.

X-ray diffraction data (8.13 g/cm$^3$). The ceramic was not well sintered as the firing temperature of 950 °C was low, compared to temperatures over 1100 °C normally used for the sintering of bulk 0.65PMN–0.35PT ceramics.[25]

### 3.3. Dielectric properties

The dielectric constants $\varepsilon$ as a function of the temperature were measured at 100 kHz for the 0.65PMN–0.35PT films on the $Al_2O_3$, Pt, 0.65PMN–0.35PT and AlN substrates and are shown in Fig. 17. The measurement of $\varepsilon(T)$ for the bulk 0.65PMN–0.35PT is added for comparison. All the samples were fired for 2 h at 950 °C. The maxima of the dielectric constants correspond to the high-temperature (HT) phase transition into the cubic phase that occurs around 170 °C, in agreement with the X-ray diffraction data (see Figs. 8, 10 and 12). Note that no dependence on the frequency was observed.

The low-temperature (LT) phase transition peaks from the monoclinic Pm to the tetragonal P4mm phases can be observed in the measurements $\varepsilon(T)$ of the 0.65PMN–0.35PT films on the alumina and platinum substrates (insets in Fig. 17) through a broad anomaly. These broad anomalies of the LT transition have maxima at around 50 °C. The temperature of this LT phase transition is in agreement with data in the literature. Alguero et al.[35] reported that the mechanical and electro-mechanical properties of 0.655PMN–0.345PT reflect the LT phase transition at 40–70 °C. Xia et al.[26] reported that $\varepsilon$ vs. temperature measurements show that the LT phase-transition peak for the non-poled 0.65PMN–0.35PT ceramics is around 50–80 °C. At first glance,

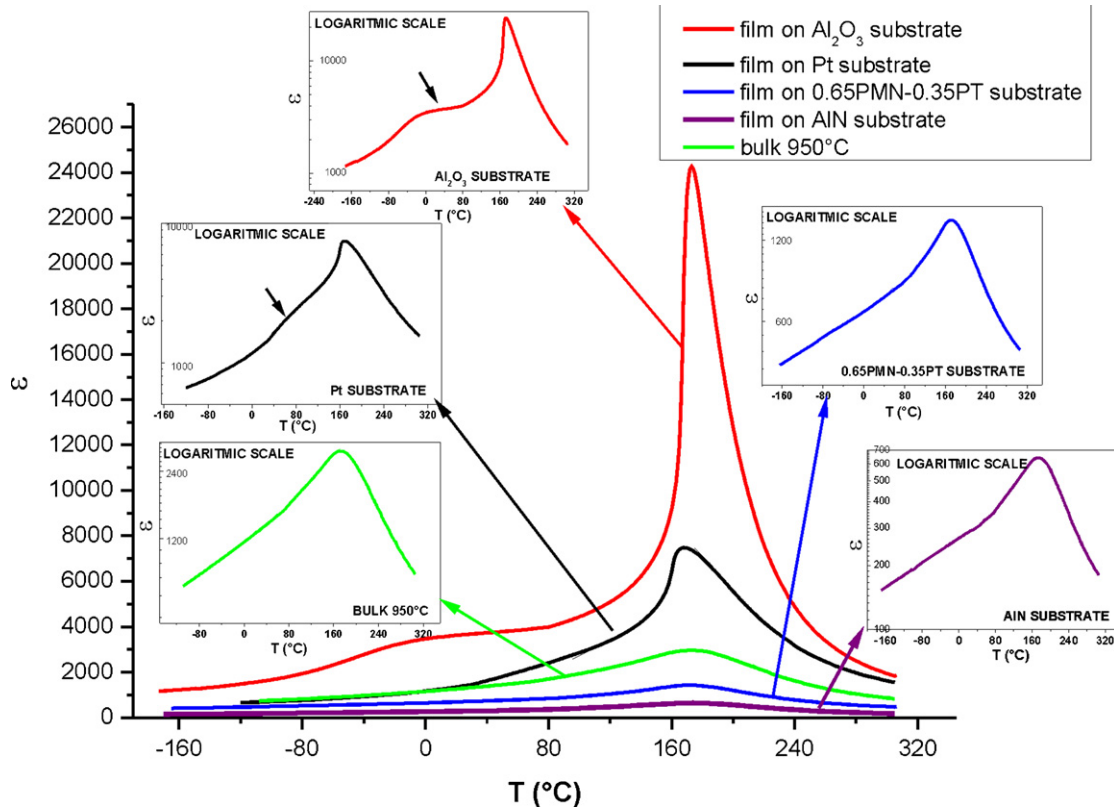Fig. 17. The $\varepsilon$ vs. temperature at 100 kHz for 0.65PMN–0.35PT films on Al$_2$O$_3$, Pt, 0.65PMN–0.35PT, AlN substrates, and for bulk ceramics. The insets show the same graphs on a logarithmic scale. The LT phase transitions are marked with black arrows.

the LT phase-transition peak is not observed for the bulk 0.65PMN–0.35PT samples and films on the 0.65PMN–0.35PT and AlN substrates. However, a kink is observed in all these previous systems at around 60 °C, which is the same temperature as in the case of the LT transition in the films on the Al$_2$O$_3$ and Pt substrates. Therefore, it seems that a small percentage of tetragonal phase may occur even in bulk 0.65PMN–0.35PT and the films on the 0.65PMN–0.35PT and AlN substrates. This corresponds to the results of the X-ray analysis of the films at different temperatures, where the possibility of the existence of the tetragonal phase exists, but the tetragonal distortion, if any, is very weak.

The highest $\varepsilon$ value at room temperature was obtained for the 0.65PMN–0.35PT films on the Al$_2$O$_3$ substrate, i.e., $\varepsilon = 3600$. The $\varepsilon$ value for the films on the Pt substrates was lower, with a value below 2000. For the films on the 0.65PMN–0.35PT and AlN substrates low values were observed, i.e., $\varepsilon = 700$ and $\varepsilon = 300$, respectively. The main reason for the differences in the $\varepsilon$ of the 0.65PMN–0.35PT thick films on the different substrates arises from the different microstructures, as shown in previous section. Indeed, the films on the 0.65PMN–0.35PT and AlN substrates show smaller grains and more porosity compared to the films deposited on the Al$_2$O$_3$ and Pt substrates.

## 4. Discussion

Thick films of 0.65PMN–0.35PT were successfully prepared on different substrates, i.e., Al$_2$O$_3$, Pt, 0.65PMN–0.35PT and AlN. All these films were screen-printed and fired under the same conditions, i.e., for 2 h at 950 °C and cooled with a rate of 3 °C/min. For comparison, the bulk 0.65PMN–0.35PT was also prepared under the same conditions.

It is possible to distinguish two kinds of substrate: Al$_2$O$_3$ and Pt, on the one hand, and 0.65PMN–0.35PT and AlN, on the other. With both Al$_2$O$_3$ and Pt, the films are well sintered, with few pores and relatively large grains ($\sim$1–2 μm), and show clear evidence of a tetragonal phase coexisting with a monoclinic phase at room temperature, which is in agreement with Ref. [23] reporting the size effect in 0.65PMN–0.35PT bulk ceramics. Under these conditions, the dielectric constants are found to be high; the highest being in the case of the Al$_2$O$_3$ substrate. In contrast, for both the 0.65PMN–0.35PT and AlN substrates the microstructure shows a smaller grain size and more pores. In addition, no tetragonal phase was detected. The dielectric constant was low, with values of less than 1000.

These results indicate that the choice of the substrate strongly influences the final characteristics of the films. The most likely explanation is that during the sintering procedure and the cooling, due to the difference in the thermal expansion coefficients (TECs) of the substrates, different residual stresses form and remain in the films. It is well known that the mechanical boundary conditions drastically affect the ferroelectric properties as the stress and the polarization are intimately coupled. This coupling is particularly strong close to the MPB[37] and especially in relaxor-based compounds.[38]

Table 3

The TEC of the substrates, the differences in TEC of the substrates and films ($\Delta$TEC = TEC$_{substrate}$ − TEC$_{film}$), the compressive or tensile stress and the phase composition in the films. The 0.65PMN–0.35PT bulk ceramics is added for comparison.

| Substrate | TEC ($\times 10^{-6}$/K) | $\Delta$TEC ($\times 10^{-6}$/K) | Stress—compression or tension | Phase composition |
|---|---|---|---|---|
| Al$_2$O$_3$ | 8[40,41] | 1.7 | Compressive | Coexistence Pm and P4mm |
| Pt | 8.8[42,43] | 2.5 | Compressive | Coexistence Pm and P4mm |
| 0.65PMN–0.35PT | 6.3 | 0 | Stress free[a] | Pm |
| AlN | 4.5[44,45] | −1.8 | Tensile[b] | Pm |
| Bulk ceramics | 6.3 | 0 | Stress free | Pm |

[a] Pt electrode is neglected.

[b] Poorly sintered and porous.

In the literature, the values for the TEC of PMN–PT single crystals with MPB compositions are reported, for the rhombohedral phase (described here as monoclinic) $4 \times 10^{-6}$/K and for the tetragonal phase $14 \times 10^{-6}$/K.[39] Our measurements of the TEC of the 0.65PMN–0.35PT bulk material showed an average value of $6.3 \times 10^{-6}$/K.

The TEC values of the Al$_2$O$_3$ and Pt substrates are around $8 \times 10^{-6}$/K[40,41] and $8.8 \times 10^{-6}$/K,[42,43] respectively, and thus are higher than the TEC of the 0.65PMN–0.35PT material, while the TEC of the AlN substrate is $4.5 \times 10^{-6}$/K[44,45] and therefore lower than the TEC of the 0.65PMN–0.35PT. In Table 3, the TECs of the substrates, the differences in the TECs of the substrates and films ($\Delta$TEC = TEC$_{substrate}$ − TEC$_{film}$), the compressive or tensile stresses and the phase compositions in the films are reported. The data for the 0.65PMN–0.35PT bulk ceramics are added for comparison.

In the case of the 0.65PMN–0.35PT films on the 0.65PMN–0.35PT substrate, the films are considered as stress free, as the Pt electrode, which is in between the substrate and film, is neglected. Both the films deposited on the Al$_2$O$_3$ and Pt substrates are under a compressive stress. In thin films, such a compressive stress favours a polarization perpendicular to the plane of the substrate, and as a consequence a tetragonal phase is favoured. For both these substrates a tetragonal phase was observed in the films. In contrast, under pure tensile stress conditions, like for the AlN substrate, the amount of tetragonal phase, if any, is very small. These findings suggest therefore that even in thick films the stress affects the properties.

To the best of our knowledge, no report on this stress effect exists for the 0.65PMN–0.35PT material. However, our results can be compared with Pb(Zr,Ti)O$_3$ (PZT) films from the literature. According to these experimental results, the compressive residual stress in PZT thin films shifts the MPB region towards the Zr-rich composition side, i.e., towards the rhombohedral phase.[7,12,13] In other words, the stress enhances the thermodynamic stability of the tetragonal phase, as would be expected under a two-dimensional compressive stress, according to the thermodynamic formalism based on the Landau–Devonshire phenomenological theory. Of course, the authors are aware that the 0.65PMN–0.35PT films are thick in comparison with the PZT thin films and that the phase diagrams for the PMN–PT and PZT materials are not similar. However, our results for 0.65PMN–0.35PT thick films under a residual stress show the same tendency as PZT thin films, i.e., the compressive stress enhances the stability of the tetragonal phase. Therefore, in addi-

tion to the grain size and the porosity in thick films, the stress conditions (residual stresses because of the process) also play a key role in the final properties of the ferroelectric thick films.

## 5. Conclusion

Thick films of 0.65PMN–0.35PT were successfully screen-printed, fired and cooled under the same conditions on different substrates (Al$_2$O$_3$, Pt, 0.65PMN–0.35PT and AlN), with the aim to study the influence of the substrates on the microstructure, the phase composition and the dielectric properties of the films.

It was demonstrated that while the process conditions are similar, drastic changes to the microstructure, the phase composition and the dielectric properties occur, depending on the substrate materials. These features might be associated with the stress felt by the thick films. Indeed, as expected from the compressive stress (the case for the Al$_2$O$_3$ and Pt substrates), 0.65PMN–0.35PT thick films exhibit a tetragonal phase in addition to the monoclinic one. These films are sintered to a high density, and both the structure and the microstructure favour a high value for the dielectric constant. In contrast, under a tensile stress, like with the AlN substrate, a monoclinic phase and rather small grains, and a higher concentration of pores, are generally observed. These results are of great interest as they show the key role played by the nature of the stress of the substrate and highlight the need to consider this parameter when designing the thick films in the devices of the future.

## Acknowledgements

## References

1. Lefki K, Dormans GJM. Measurement of piezoelectric coefficients of ferroelectric thin films. *J Appl Phys* 1994;**76**:1764–7.
2. Setter N, Damjanovič D, Eng L, Fox G, Gevorgian S, Hong S, et al. Ferroelectric thin films: review of materials, properties, and applications. *J Appl Phys* 2006;**100**(051606):1–46.
3. Damjanovič D. Ferroelectric, dielectric and piezoelectric properties of ferroelectric thin films and ceramics. *Rep Prog Phys* 1998;**61**:1267–324.
4. Dawber M, Rabe KM, Scott JF. Physics of thin-film ferroelectric oxides. *Rev Mod Phys* 2005;**77**:1083–130.
5. Gentil S, Damjanovic D, Setter N. Pb(Mg$_{1/3}$Nb$_{2/3}$)O$_3$ and $(1 − x)$Pb(Mg$_{1/3}$Nb$_{2/3}$)O$_3$–$x$PbTiO$_3$ relaxor ferroelectric thick

films: processing and electrical characterization. *J Electroceram* 2004;**12**:151–61.

6. Kosec M, Holc J, Kuščer D, Drnovšek S. $Pb(Mg_{1/3}Nb_{2/3})O_3$–$PbTiO_3$ thick films from mechanochemically synthesized powder. *J Eur Ceram Soc* 2007;**27**:2778–3775.

7. Oh SH, Jang HM. Enhanced thermodynamic stability of tetragonal-phase field in epitaxial $Pb(Zr,Ti)O_3$ thin films under a two-dimensional compressive stress. *Appl Phys Lett* 1998;**72**:1457–559.

8. Oh SH, Jang HM. Two-dimensional thermodynamic theory of epitaxial $Pb(Zr,Ti)O_3$ thin films. *Phys Rev B* 2000;**62**:14757–65.

9. Oh SH, Jang HM. Epitaxial $Pb(Zr,Ti)O_3$ thin films with coexisting tetragonal and rhombohedral phases. *Phys Rev B* 2001;**62**(132101):1–4.

10. Pertsev NA, Kukhar VG, Kohlstedt H, Waser R. Phase diagrams and physical properties of single-domain epitaxial $Pb(Zr_{1-x}Ti_x)O_3$ thin films. *Phys Rev B* 2003;**67**:1–10, 054107.

11. Kanno I, Yokoyama Y, Kotera H. Thermodynamic study of *c*-axis-oriented epitaxial $Pb(Zr,Ti)O_3$ thin films. *Phys Rev B* 2004;**69**(064103):1–7.

12. Lee K, Baik S. Morphotropic phase boundary in epitaxial $Pb(Zr,Ti)O_3$ thin films: two-dimensional planar size effect. *Appl Phys Lett* 2005;**86**:1–3, 20290.

13. Sakamaki Y, Fukazawa H, Wakiya N, Suzuki H, Shinozaki K, Ohno T, et al. Effect of film thickness on electrical properties of chemical solution deposition-derived $Pb(Zr_xTi_{1-x})O_3/LaNiO_3/Si$. *J Appl Phys* 2007;**46**:6925–8.

14. Kornev IA, Bellaiche L, Janolin P-E, Dkhil B, Suard E. Phase diagram of $Pb(Zr,Ti)O_3$ solid solutions from first principles. *Phys Rev Lett* 2006;**97**(157601):1–4.

15. Koo TY, Cheong SW. Dielectric and piezoelectric enhancement due to $90°$ domain rotation in the tetragonal phase of $Pb(Mg_{1/3}Nb_{2/3})O_3$–$PbTiO_3$. *Appl Phys Lett* 2002;**80**:4205–7.

16. Alguero M, Moure A, Pardo L, Holc J, Kosec M. Processing by mechanosynthesis and properties of piezoelectric $Pb(Mg_{1/3}Nb_{2/3})O_3$–$PbTiO_3$ with different compositions. *Acta Mater* 2006;**54**:501–11.

17. Kelly J, Leonard M, Tantigate C, Safari A. Effect of composition on the electromechanical properties of $(1-x)Pb(Mg_{1/3}Nb_{2/3})O_3$–$xPbTiO_3$ ceramics. *J Am Ceram Soc* 1997;**80**:957–64.

18. Singh AK, Pandey D. Evidence for $M_B$ and $M_C$ phases in the morphotropic phase boundary region of $(1-x)[Pb.Mg_{1/3}Nb_{2/3}O_3]$–$xPbTiO_3$: a Rietveld study. *Phys Rev B* 2003;**67**(064102):1–12.

19. Noheda B, Cox DE, Shirane G, Park S-E, Cross LE, Zhong Z. Polarization rotation via a monoclinic phase in the piezoelectric $92\%PbZn_{1/3}Nb_{2/3}O_3$–$8\%PbTiO_3$. *Phys Rev Lett* 2001;**86**:3891–4.

20. Singh AK, Pandey D. Structure and the location of the morphotropic phase boundary region in $(1-x)[Pb(Mg_{1/3}Nb_{2/3})O_3]$–$xPbTiO_3$. *J Phys: Condens Matter* 2001;**13**:L931–6.

21. Kiat JM, Uesu Y, Dkhil B, Matsuda M, Malibert C, Calvarin G. Monoclinic structure of unpoled morphotropic high piezoelectric PMN–PT and PZN–PT compounds. *Phys Rev B* 2002;**65**(064106):1–4.

22. Noheda B, Cox DE, Shirane G, Gao J, Ye Z-G. Phase diagram of the ferroelectric relaxor $(1-x)Pb(Mg_{1/3}Nb_{2/3})O_3$–$xPbTiO_3$. *Phys Rev B* 2002;**66**:1–10, 054104.

23. Alguero M, Ricote J, Jimenez R. Size effect in morphotropic phase boundary $Pb(Mg_{1/3}Nb_{2/3})O_3$–$PbTiO_3$. *Appl Phys Lett* 2007;**91**:1–3, 112905.

24. Carreaud J, Gemeiner P, Kiat JM, Dkhil B, Bogicevic C, Rojac T, et al. Size-driven relaxation and polar states in $PbMg_{1/3}Nb_{2/3}O_3$-based system. *Phys Rev B* 2005;**72**:1–6, 174115.

25. Leite ER, Scotch AM, Khan A, Chan H, Harmer MP. Chemical heterogeneity in PMN–35PT ceramics in effects on dielectric and piezoelectric properties. *J Am Ceram Soc* 2002;**85**:3018–24.

26. Xia Z, Wang L, Yan W, Li Q, Zhang Y. Comparative investigation of structure and dielectric properties of $Pb(Mg_{1/3}Nb_{2/3})O_3$–$PbTiO_3$ (65/35) and 10% $PbZrO_3$-doped $Pb(Mg_{1/3}Nb_{2/3})O_3$–$PbTiO_3$ (65/35) ceramics prepared by a modified precursor method. *Mater Res Bull* 2007;**42**:1715–22.

27. Gentil S, Damjanovic D, Setter N. Development of relaxor ferroelectric materials for screen-printing on alumina and silicon substrates. *J Eur Ceram Soc* 2005;**25**:2125–8.

28. Kuščer D, Skalar M, Holc J, Kosec M. Processing and properties of $0.65Pb(Mg_{1/3}\ Nb_{2/3})O_3$–$0.35PbTiO_3$ thick films. *J Eur Ceram Soc* 2009;**29**:105–13.

29. Uršič H, Hrovat M, Holc J, Zarnik MS, Drnovšek S, Maček S, et al. A large-displacement $65Pb(Mg_{1/3}Nb_{2/3})O_3$–$35PbTiO_3/Pt$ bimorph actuator prepared by screen printing. *Sens Actuators B: Chem* 2008;**133**:699–704.

30. Uršič H, Škarabot M, Hrovat M, Holc J, Skalar M, Bobnar V, et al. The electrostrictive effect in ferroelectric $0.65Pb(Mg_{1/3}Nb_{2/3})O_3$–$0.35PbTiO_3$ thick films. *J Appl Phys* 2000;**103**:1–4, 124101.

31. Kosec M, Holc J, Malič B, Bobnar V. Processing of high performance lead lanthanum zirconate titanate thick films. *J Eur Ceram Soc* 1999;**19**:949–54.

32. Holc J, Hrovat M, Kosec M. Interactions between alumina and PLZT thick films. *Mater Res Bull* 1999;**34**:2271–8.

33. *The crystallographic computing system*. Praha, Czech Republic: Institute of Physics; 2006.

34. Uršič H, Tellier J, Hrovat M, Holc J, Drnovšek S, Bobnar V, et al., The effect of poling on the properties of $0.65Pb(Mg_{1/3}Nb_{2/3})O_3$–$0.35PbTiO_3$ ceramics. J Appl Phys; in press.

35. Alguero M, Alemany C, Pardo L, Thi MP. Piezoelectric resonances, linear coefficients and losses of morphotropic phase boundary $Pb(Mg_{1/3}Nb_{2/3})O_3$–$PbTiO_3$ ceramics. *J Am Ceram Soc* 2005:1–8, 00.

36. Dkhil B, Defay E, Guillan J. Strains in $BaTiO_3$ thin film deposited onto Pt-coated Si substrate. *Appl Phys Lett* 2007;**90**:1–3, 022908.

37. Park SE, Shrout TR. Ultrahigh strain and piezoelectric behavior in relaxor based ferroelectric single crystals. *J Appl Phys* 1997;**82**:1804–11.

38. Dkhil B, Gemeiner P, Al-Barakaty A, Bellaiche L, Dul'kin E, Mojaev E, et al. Intermediate temperature scale T* in lead-based relaxor systems. *Phys Rev B* 2009;**80**(064103):1–6.

39. Sehirlioglu A, Payne DA, Han P. Thermal expansion of phase transformations in $(1-x)Pb(Mg_{1/3}Nb_{2/3})O_3$–$xPbTiO_3$: evidence for preferred domain alignment in one of the $\langle 0\,0\,1\rangle$ directions for melt-grown crystals. *Phys Rev B* 2005;**72**:1–5, 214110.

40. http://www.marketech-alumina.com/.

41. http://emtoolbox.nist.gov/Temperature/Slide14.asp.

42. Lide DR. *Handbook of chemistry and physics*. 86th ed. Broken Sound Parkway, NW: Taylor & Francis Group; 2005–2006. p. 12–197.

43. http://en.wikipedia.org/wiki/Coefficient_of_thermal_expansion.

44. Li J, Wei P, Qiliang H, Chen J, Zhang Z. Mechanism of titanium deposition on AlN surface by molten salt reaction. *Mater Lett* 2003;**57**:1369–73.

45. Zhu S, Wlosinski W. Joining of AlN ceramic to metals using sputtered Al or Ti film. *J Mater Process Technol* 2001;**109**:277–82.